PHYSICAL REVIEW C VOLUME 18, NUMBER 6 DECEMBER 1978

β-γ angular correlation in ^{20}F: The second class current problem

R. E. Tribble and D. P. May
Cyclotron Institute, Texas A&M University, College Station, Texas 77843
(Received 15 May 1978)

The β-γ angular correlation in the decay of ^{20}F has been measured using a symmetric four detector system and an activated LiF target. ^{20}F was produced by the ^{19}F$(d,p)^{20}$F reaction using a low-energy deuteron beam ($E_d = 2$ MeV). Correlation data were acquired for $\theta_{\beta\text{-}\gamma} = 90°$ and $\theta_{\beta\text{-}\gamma} = 180°$ and these data were anlayzed for systematic differences as a function of electron energy (E_β). We report a corrected first order slope to the ratio of β spectra $N(180°)/N(90°)$ of $(+0.5 \pm 0.7)10^{-3}$ (MeV)$^{-1}$, with an intercept for this ratio of 1.001 ± 0.002. Incorporating this value for the slope with other data on the $A = 20$ system, we find an upper limit for the second class current contribution to the correlation which is less than 1/3 of the contribution of weak magnetism and consistent with zero.

[RADIOACTIVITY ^{20}F; measured β-γ angular correlation. Determined induced weak currents.]

I. INTRODUCTION

A number of experiments have been performed recently to test for nuclear induced weak currents. At issue are the "strong form" of the conserved vector current hypothesis (CVC),[1] which relates the vector β decay interaction to the electromagnetic interaction, and the possible presence of a second class current (SCC).[2] These induced interactions are quite small being recoil order corrections, and typically are reduced in strength, compared to allowed β decay, by $\sim E_\beta/m_n c^2$, where E_β is the β energy and m_n the nucleon mass. In order to study these recoil order interactions, it is necessary to isolate them from the dominant allowed transitions. Theoretical calculations of the β decay spectrum indicate that correlation measurements are best suited to study such induced interactions.[3]

Both CVC and the presence or absence of a SCC interaction play an important role in determining the symmetry properties of the charged weak hadronic interaction. With the advent of unified gauge theories of the weak and electromagnetic interactions, a complete accounting of the weak interaction symmetry properties becomes crucial. CVC follows naturally from the gauge theories.[4] However, an SCC interaction is difficult, if not impossible, to accomodate in all of the theories proposed.[5]

In addition to testing gauge theories, confirmation of CVC provides a powerful tool for the analysis of β spectra. Via CVC, all of the weak vector currents can be predicted from the analog electromagnetic processes which can typically be measured to high precision. β decay experiments can then focus on determining the character of the axial vector interaction which has no electromagnetic analog.

To date the best test of CVC is the comparison of the weak magnetism interaction, determined from the β spectrum shapes in $A = 12$, to the analog $M1$ γ decay.[6] Changes in the nuclear masses, γ decay width, and branching ratios have prompted a reevaluation of the results,[7] although the most recent analysis still finds good agreement with CVC.[8] A number of experiments sensitive to induced interactions have been performed in $A = 8$ with the results consistent with CVC and no SCC.[9] In both $A = 12$ (Ref. 10) and $A = 19$ (Ref. 11), β asymmetry measurements from polarized parents have suggested a large SCC interaction. However, a recent experiment in $A = 12$ with aligned initial states is consistent with no SCC.[12] We note that this new experiment is a more sensitive test of an SCC since there are no allowed contributions to the asymmetry measured from an alignment. Hence a nonzero result should only arise from induced currents. In the polarization experiment, however, there is an allowed contribution which produces an asymmetry independent of induced currents. Thus with the new result in $A = 12$, the only remaining evidence for an SCC is in $A = 19$.[13]

In order to provide additional experimental information on induced currents, we report below a new measurement of the ^{20}F β-γ angular correlation. The relevant decay scheme is shown in Fig. 1. The ^{20}F decay is an allowed $2^+ \rightarrow 2^+$ transition to the first excited state of ^{20}Ne ($E_x = 1.63$ MeV), which subsequently undergoes an $E2$ γ decay. For reference, the ^{20}Na decays are also given in Fig.

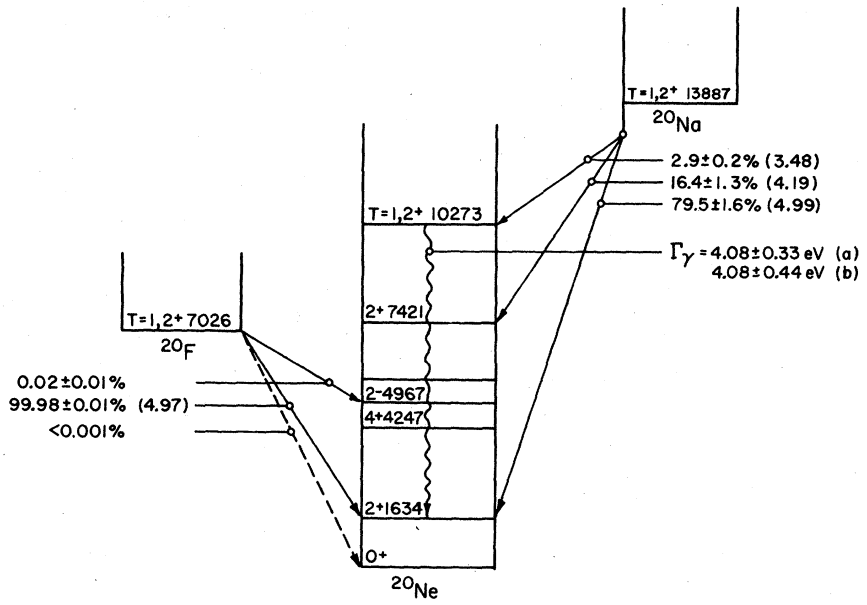

FIG. 1. Decay scheme for the $A=20$ system. Numbers in parentheses are log (ft) values. Excitation energies, branching ratios, and log (ft) values are from Ref. 26. The γ widths quoted are from Ref. 18 for (a) and Ref. 19 for (b).

1. We note that there is a high probability for ^{20}Na to decay to the lowest 2^+ level in ^{20}Ne. Also the additional ^{20}Na decays populate final states that subsequently α decay. The results of a measurement of the ^{20}Na β-γ correlation, which has been reported recently, is given in Table I. In addition the table contains the most recent results for the ^{20}F and ^{20}Na ft values, the analog $M1$ γ decay width and $E2/M1$ mixing ratio, and results of previous β-γ correlation measurements for ^{20}F. The com-

TABLE I. β and γ-decay measurements in $A=20$.

β-γ angular correlations	B (10^{-3} MeV^{-1})	C (10^{-4} MeV^{-2})
^{20}F [a]	+2.0±0.6	...
^{20}F [b]	+0.9±0.7	...
^{20}F [c]	+0.2±0.2	...
^{20}Na [d]	−4.0±0.7	+1.3±0.9
Analog γ ray		
$M1$ decay width Γ_{M1} [e,f]	4.08±0.33, 4.08±0.44 eV	
$E2/M1$ mixing ratio [g]	0.00039	
β strength to 2^+		
(E_x=1.63 MeV) state in ^{20}Ne	logft	
^{20}F [h]	4.972±0.001	
^{20}Na [i]	4.986±0.010	

[a] Reference 14. Measured at $E_\beta \simeq 5$ MeV.
[b] Reference 15. Least squares fit (LSF) to $A+BE_\beta$.
[c] Reference 16. LSF to $1.0+BE_\beta$.
[d] Reference 17. LSF to $1.0+BE_\beta+CE_\beta^2$.
[e] Reference 18.
[f] Reference 19.
[g] Reference 20.
[h] Reference 21.
[i] Reference 22.

plete set of electromagnetic measurements will be utilized below to predict, via CVC, the vector interaction contributions to the β-γ correlation. Assuming CVC, a comparison of the ^{20}F and ^{20}Na correlations will determine the strength of the SCC interaction in $A=20$.

II. THE ANGULAR CORRELATION

There have been several extensive theoretical calculations of the correlation effects of allowed β decay. We choose to adopt the elementary particle approach, recently reviewed by Holstein.[3] The assumed interaction is the usual (V-A) current-current interaction. The decay amplitude T for the decay $\alpha \rightarrow \beta + e^- + \bar{\nu}$ is

$$T=\frac{G_V}{\sqrt{2}}\cos\theta_C\langle\beta|[V_\mu(0)+A_\mu(0)]|\alpha\rangle l^\mu \ , \tag{1}$$

where α (β) is the initial (final state), G_V the vector coupling constant, θ_C the Cabibbo angle, l^μ the lepton current, and V_μ (A_μ) the vector (axial vector) nucleon current. The decay amplitude has been calculated by Holstein to second order in recoil. The dominant Coulomb effects are included via a Fermi function. Additional electromagnetic corrections are typically small and will be ignored.

The spectrum for the $A=20$ β-γ correlation, integrated over neutrino variables is

$$dW=F_\pm(Z,E)G_V{}^2\cos^2\theta_C(E_0-E)^2pE dE d\Omega_e d\Omega_\gamma \times\left\{f_1(E)+f_2(E)\left[\left(\frac{\hat{K}\cdot\vec{p}}{E}\right)^2-\frac{1}{3}\frac{p^2}{E^2}\right]\right\}, \tag{2}$$

where $F_\pm$ is the Fermi function, E (E_0) the electron energy (end point energy), $\hat{K}$ a unit vector in the direction of the γ, and $\vec{p}$ the electron momentum. A term proportional to $\hat{K}\cdot\vec{p}/E$, which arises from the transformation from the laboratory to the c.m. frame of the daughter, is quite small for β-γ correlations and hence is neglected. The spectral functions $f_1(E)$ and $f_2(E)$ to second order in recoil for the $A=20$ decays are

$$f_1(E)=c^2-\frac{2}{3}\frac{E_0}{M}[c^2\pm c(b+d)]+\frac{2}{3}\frac{E}{M}(5c^2\pm 2cb) -\frac{1}{3}\frac{m_e{}^2}{ME}\left[2c^2\pm c(2b+d)-\frac{E_0-E}{2M}ch\right], \tag{3}$$

$$f_2(E)=\frac{E}{2M}\left\{c^2\pm c(b-d) -\frac{1}{\sqrt{14}}\left[\pm\left(\frac{3}{2}\right)^{1/2}\frac{(E_0-E)}{M}cg\pm 3cf +\frac{3cj_2(E_0-2E)}{2M}\right] -\frac{3cj_3}{\sqrt{35}}\left(\frac{E}{M}\right)\right\}, \tag{4}$$

where the upper (lower) sign refers to electron (positron) decay. The form factors defined in Eqs. (3) and (4) are commonly known as Gamow-Teller (c), weak magnetism (b), induced tensor (d), pseudoscalar (h), second forbidden vector (f and g), and second forbidden axial vector (j_2 and j_3). The induced tensor form factor d can have both first and second class components according to $d=d_{\rm I}\pm d_{\rm II}$. The other axial vector form factors c, h, j_2, and j_3 could also contain both first and second class contributions, but in all cases the first class part is expected to dominate these form factors. CVC restricts b, f, and g to be only first class.

The form factors defined above are related to nuclear matrix elements by the impulse approximation. To lowest order, they are

$$b=A\left[g_V\left\langle\beta\left|\left|\sum_i\tau_i\vec{L}_i\right|\right|\alpha\right\rangle+g_m\left\langle\beta\left|\left|\sum_i\tau_i\vec{\sigma}_i\right|\right|\alpha\right\rangle\right], \tag{5a}$$

$$c=g_A\left\langle\beta\left|\sum_i\tau_i\vec{\sigma}_i\right|\right|\alpha\right\rangle, \tag{5b}$$

$$d_{\rm I}=Ag_A\left\langle\beta\left|\left|\sum_i\tau_i\vec{\sigma}_i\times\vec{L}_i\right|\right|\alpha\right\rangle, \tag{5c}$$

$$f=(\tfrac{2}{3})^{1/2}M\Delta g_V\left(\frac{4\pi}{5}\right)^{1/2}\left\langle\beta\left|\left|\sum_i\tau_i r_i{}^2Y_2(\hat{r}_i)\right|\right|\alpha\right\rangle, \tag{5d}$$

$$g=-\tfrac{4}{3}M^2g_V\left(\frac{4\pi}{5}\right)^{1/2}\left\langle\beta\left|\left|\sum_i\tau_i r_i{}^2Y_2(\hat{r}_i)\right|\right|\alpha\right\rangle, \tag{5e}$$

$$j_K=-\tfrac{2}{3}M^2g_A\left(\frac{4\pi}{5}\right)^{1/2} \times\left\langle\beta\left|\left|\sum_i\tau_i r_i{}^2[\vec{\sigma}_i,\vec{Y}_2(\hat{r}_i)]^k\right|\right|\alpha\right\rangle, \tag{5f}$$

where Δ is the parent-daughter mass difference, M the parent mass, A the nuclear number, $g_V=1$, $g_A=1.23$, and $g_m=4.7$ and is the difference between the neutron and proton nuclear moments. The second class form factor $d_{\rm II}$ does not have a simple impulse-approximation prediction since the axial current is not divergenceless.[23] Calaprice *et al.*[24] have calculated the form factors in Eq. (5) for $A=20$ using $(sd)^8$ configuration shell model wave functions.

The form factor $|c|$ can be found from the ft value of Table I by

$$c^2=\frac{6165}{ft} \ . \tag{6}$$

Using the quoted ^{20}F value, we find $c=0.256\pm 0.006$. CVC relates the form factor b to the $M1$ γ transition according to[3]

$$|b| = \left(\frac{6\Gamma_{M1}M^2}{\alpha E_\gamma{}^3}\right)^{1/2}, \tag{7}$$

where $\alpha = 1/137$, E_γ is the γ energy, Γ_{M1} the isovector $M1$ width, and M the nuclear mass. Again using the values in Table I, we find $b = 42.7 \pm 1.2$, and thus $b/Ac = 8.34 \pm 0.30$. CVC also relates the form factors f and g to the $E2$ γ width. The $E2/M1$ mixing ratio combined with Γ_{M1} gives $\Gamma_{E2} \simeq 1.6 \times 10^{-3}$ eV. The form factor g is then[3]

$$|g| = \frac{3}{4}\left(\frac{(30)\Gamma_{E2}M^4}{\alpha E_\gamma{}^2}\right)^{1/2} \simeq 3085 . \tag{8}$$

The impulse approximation results suggest that g is negative, and thus we set $g \simeq -3085$. The form factor f is related to g by

$$f = -\left(\frac{3}{2}\right)^{1/2}\frac{\Delta}{2M}g \simeq 0.9 . \tag{9}$$

The estimates for f and g agree reasonably well with the wave function calculations and suggest that these form factors provide negligible contributions to the correlation.

From Eq. (2) we expect the experimental angular correlation to be of the form

$$W_\pm(\theta_{\beta\gamma}) = 1 + p_\pm \cos^2\theta_{\beta\gamma} , \tag{10}$$

where

$$p = \frac{f_2(E)}{f_1(E) - \frac{1}{3}f_2(E)} . \tag{11}$$

As we noted above, the f and g form factors are expected to be small and shall be ignored. In addition, the energy dependent terms in the denominator of Eq. (11) contribute only a few percent to p, and thus they too shall be ignored. The coefficient p is then

$$p_\pm \simeq \frac{E}{4m_nAc}\left[1 \pm b \mp d_{II} - d_I - \frac{3}{2\sqrt{14}}\frac{j_2}{m_nA}(E_0 - 2E) - \frac{3}{\sqrt{35}}\frac{j_3}{m_nA}E\right] . \tag{12}$$

The G-parity transformation property can be utilized to help separate the b and d_{II} form factors from d_I, j_2, and j_3. Combining the ^{20}F and ^{20}Na correlations yields

$$p(^{20}\mathrm{F}) - p(^{20}\mathrm{Na}) = \frac{E}{2m_nAc}\left[b - d_{II} + \frac{3}{2\sqrt{14}}\frac{j_2}{m_nA}\Delta(E_0)\right] , \tag{13}$$

where $\Delta(E_0) = E_0(^{20}\mathrm{Na}) - E_0(^{20}\mathrm{F}) = 5.8$ MeV. The nonzero result for $\Delta(E_0)$ indicates that j_2 cannot be neglected in extracting a result for d_{II}. Also we note that

$$p(^{20}\mathrm{F}) + p(^{20}\mathrm{Na}) = \frac{E}{2m_nAc}\left[1 - d_I + \frac{3}{\sqrt{14}}\frac{j_2E}{m_nA} - \frac{3}{2\sqrt{14}}\frac{j_2}{m_nA}\Delta'(E_0) - \frac{3}{\sqrt{35}}\frac{j_3}{m_nA}E\right] , \tag{14}$$

where $\Delta'(E_0) = E_0(^{20}\mathrm{F}) + E_0(^{20}\mathrm{Na})$. Thus the first class induced tensor d_I can be investigated by combining the results as in Eq. (14). Extracting d_I will require a careful reckoning of j_2 and j_3, however.

III. EXPERIMENTAL PROCEDURE

The experiment was performed at the Rice University Tandem Van de Graaff Accelerator. ^{20}F was produced at the center of the detection chamber by the ^{19}F$(d,p)^{20}$F reaction with $E_d = 2$ MeV. The deuteron beam impinged on a target of 200 μg/cm^2 ^{6}LiF enriched to 96% ^{6}Li on a 900 μg/cm^2 Ni backing. ^{7}Li material was avoided in order to minimize the β background from the decay of ^{8}Li which would be produced by the ^{7}Li$(d,p)^8$Li reaction. The target was positioned in the center of the chamber by a thin aluminum rod so that the LiF material faced the beam. The beam was collimated before entering the detection chamber producing an 8 mm^2 beam spot on target.

The detection geometry is shown in Fig. 2. Four detectors, two β and two γ detectors, were positioned in a plane perpendicular to the beam axis and at right angles to one another. Each β detector consisted of a cylindrical (7.62 cm $\times$ 7.62 cm) plastic scintillator mounted in the chamber vacuum and optically coupled to a phototube via an ultraviolet transparent, acrylic light pipe. A lead collimator was placed over each scintillator so that electrons could enter the scintillator only through a 3.81 cm diameter circular aperture. The two 7.62 cm $\times$ 7.62 cm NaI(Tl) γ detectors were positioned outside the chamber so that γ rays coming from the source travelled through the aluminum wall of the chamber before entering the γ detectors. The β and γ detectors encompassed 0.162 sr and 0.391 sr of solid angle, respectively.

The electronics are illustrated by Fig. 3. A programmable timer was used to control a mechanical beam chopper and to gate the electronics. Signals corresponding to the γ ray energy were routed through a gain stabilizer to prevent signal drifts over long counting periods. Pulses corresponding to the arrival of a signal from one of the γ detectors were delayed with respect to the other. The two signals were then summed and used as the stop for a time to amplitude converter (TAC). The β detectors provided the start signal for the TAC's and the delay in the γ signals provided two

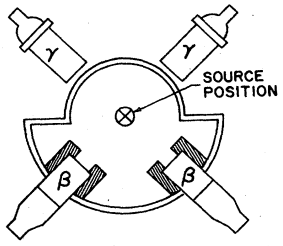

FIG. 2. Detector geometry: The beam direction is into the page.

separate timing peaks to distinguish between the two possible coincidences.

Data acquisition was divided into twelve second cycles. For six seconds the timer provided a dc gate which interrupted signals going to the ADC's while the deuteron beam was allowed to strike the target. For six seconds thereafter, the beam was interrupted well upstream from the detection chamber by the mechanical chopper, during which time data were acquired from the activated target. The beam current on target was kept low (~20 nA), and the twelve second cycles were chosen so that there could be a fairly constant rate of data acquisition in order to minimize signal pile-up. 2×10^4 coincidences per hour was a typical rate. Total running time was approximately eight days. The data were event-mode recorded on magnetic tape. Each acquired event consisted of β energy, γ energy, and fast-timing (TAC) signals from the four possible β-γ coincidences. In addition, each acquired event was labeled with a tag corresponding to one of the β detectors. To allow for differences in counting efficiencies, the positions of the two γ detectors were interchanged periodically so that each β-γ pair would be used to acquire data for both $\theta_{\beta\gamma}=90°$ and 180°. In addition, halfway between each interchange of γ detectors, the stop signals to the TAC's were interchanged. Typical β and γ spectra thus acquired are shown in Fig. 4.

IV. DATA ANALYSIS AND EXPERIMENTAL RESULTS

All data analysis was performed offline. Spectra were built up from the event mode tape in various ways in order to investigate background contributions. In the singles spectra for γ rays a peak due to the 1.779 MeV γ ray from the decay of an excited state of ^{28}Si was present on the high energy side of the 1.63 MeV γ peak as shown by Fig. 4. The relative yield of these ^{28}Si γ's was approximately 1%. In γ spectra of the coincidence data, no peak due to the ^{28}Si γ decay could be discerned. Background in the TAC spectra was low ($\sim10^{-2}$ below the TAC peaks) so that accidental β-γ coincidences were judged to be negligible, and no background subtraction was performed on the TAC spectra.

β coincidence spectra were built up from the event mode tape by setting windows corresponding

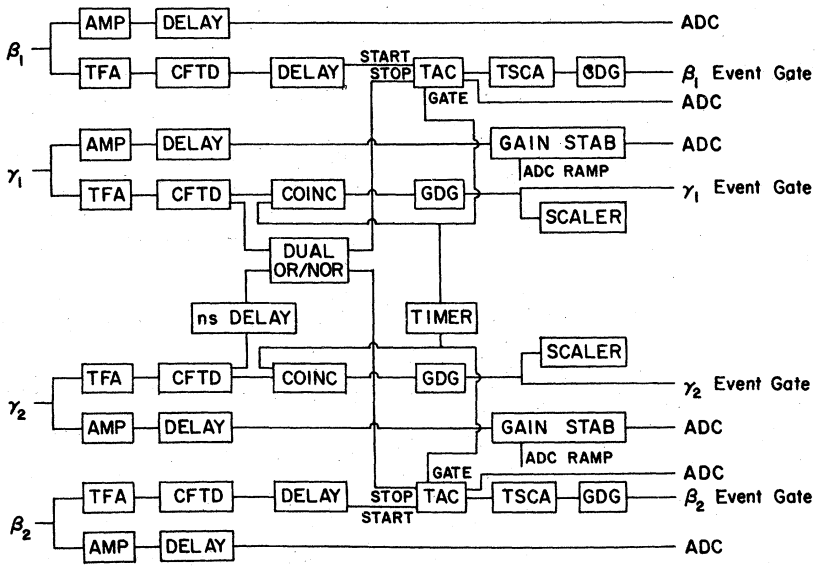

FIG. 3. The electronics setup: Boxes refer to amplifiers (AMP), timing filter amplifiers (TFA), constant fraction discriminators (CFTD), logic amplifiers (COINC and DUAL OR/NOR), time-to-amplitude converters (TAC), gate and delay amplifiers (GDG), timing single channel amplifiers (TSCA), and digital gain stabilizers (GAIN STAB).

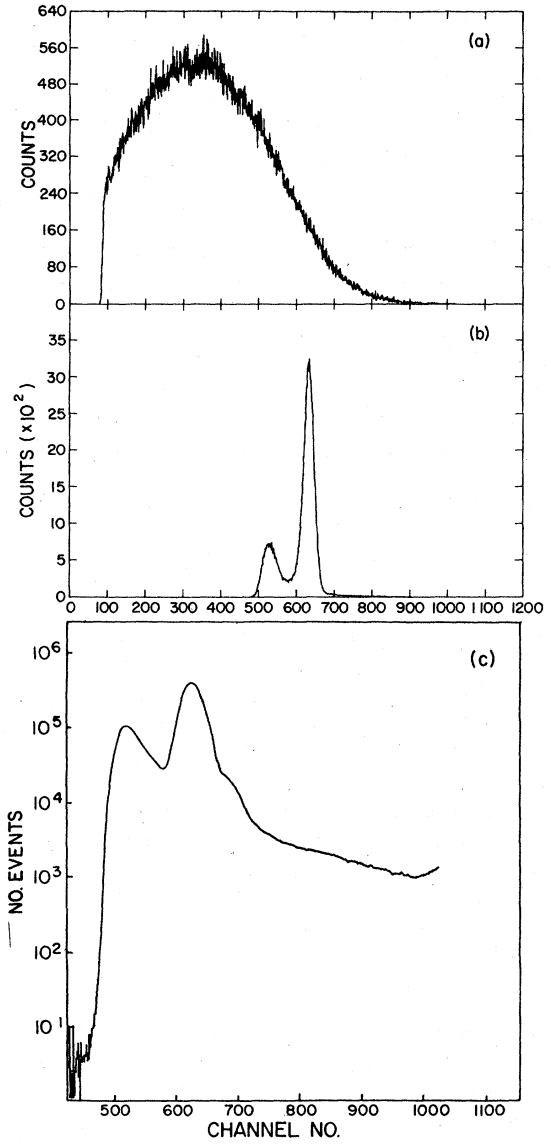

FIG. 4. Event spectra for (a) β's and (b) γ's in coincidence. (c) A typical γ singles spectrum (the ^{28}Si peak is noticeable at channel No. 700). On both γ spectra the Compton edge is just above a lower level discriminator cutoff.

to the proper tags, acceptable TAC signals, and acceptable γ energies. An effort was made to generate asymmetric effects between β coincidence spectra by varying the γ energy windows and TAC windows. It was found that since the TAC signals did indeed exhibit a slight pulse height dependence, it was possible to generate appreciable false asymmetries with narrow TAC windows. After individual coincidence spectra had been built up satisfactorily, they were next energy calibrated by Kurie plots so that the spectra of different runs could then be combined. A typical Kurie plot is shown in Fig. 5.

The data were analyzed by performing least squares fits to the quantity $N(180°)/N(90°)$ as a function of E_β where $N(\theta)$ represents the β spectrum corresponding to β-γ coincidences at the angle θ. Also as a check, least squares fit to the quantity

$$[N_1(180°)N_2(180°)/N_1(90°)N_2(90°)]^{1/2}$$

were performed where the subscripts refer to the two tags identifying the two β detectors to the computer. The $N(\theta)$ were calculated for various energy steps, and it was found that a least squares fit to the data was sensitive to the calibration of these steps when they were chosen too large. As a consequence, the steps were kept small (25 keV) in the final fitting of the data, although a sample straight line fit utilizing larger steps is illustrated in Fig. 6. The range of E over which fits were made was chosen to be 1400–5000 keV.

Parametrizing $N(180°)/N(90°)$ by $A+BE_\beta$, the least squares fit gives $A=1.001\pm0.002$ and $B=(+0.40\pm0.6)\times10^{-3}$ MeV^{-1} with a χ^2 per degree of freedom (χ_R^2) equal to 0.90. A least squares fit to the second order form $A+BE_\beta+CE_\beta^2$ gives $A=1.002\pm0.005$, $B=(-0.6\pm3.9)\times10^{-3}$ MeV^{-1}, and $C=(+0.1\pm0.6)\times10^{-3}$ MeV^{-2} with $\chi_R^2=0.91$. Parametrizing $N(180°)/N(90°)$ by $1.0+BE_\beta$, i.e., requiring the ratio to be unity for $E=0$, the least squares fit yields $B=(+0.8\pm0.2)\times10^{-3}$ MeV^{-1} with $\chi_R^2=0.88$. The second order fit to $1.0+BE_\beta+CE_\beta^2$ gives $B=(+1.1\pm0.7)\times10^{-3}$ MeV^{-1} and $C=(-0.1\pm0.2)\times10^{-3}$ MeV^{-2} with $\chi_R^2=0.90$. Parametrizing

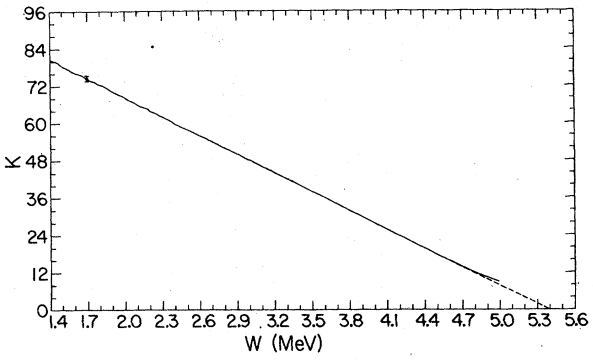

FIG. 5. Typical Kurie plot for a block of data. The solid line connects the data points and the dashed line is the detector calibration curve. No correction for finite detector resolution is included. The uncertainty in K is shown by the error bar at 1.7 MeV. Above 2.4 MeV the uncertainty is of the order of the line width.

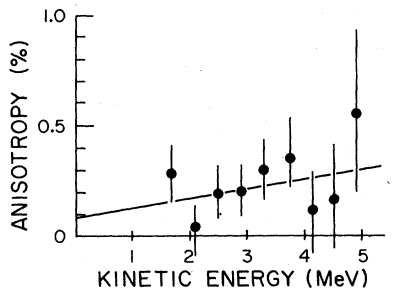

FIG. 6. Linear least squares fit to the correlation data. Note that the vertical scale is quite expanded.

$[N_1(180°)N_2(180°)/N_1(90°)N_2(90°)]^{1/2}$

by $A+BE_\beta$ gives $A=1.001\pm0.002$ and $B=(+0.5\pm0.6)\times10^{-3}$ MeV^{-1} with a $\chi_R^2=0.99$. Due to the possibility of unequal detector efficiencies, the zero energy intercept should be kept as a free parameter. However, the data clearly do not allow the determination of a second order term with any precision. Therefore with the assumption that the anisotropy is linear to a reasonable approximation over this energy range, the value for B obtained in the two parameter fit to $N(180°)/N(90°)$ is used in what follows. The effect of a small quadratic term is explored in detail below.

As an additional check on the data, β coincidence spectra were formed using those events which contained a γ energy signal in the Compton scattering region. These data yeilded a reasonable linear fit with a value for B consistent with the value quoted above which used events containing γ energies within the photopeak.

Finally the value for B obtained in the two parameter fit to $N(180°)/N(90°)$ was corrected for finite angular acceptance and β energy resolution. Incorporating these corrections, the value for B becomes $(+0.5\pm0.7)\times10^{-3}$ MeV^{-1}. Systematic effects such as β bremsstrahlung and electron source scattering were estimated and found not to be important contributions to the observed slope. The experimental arrangement is such that electron scattering will not produce an anisotropy. The β bremsstrahlung probability, combined with the effective γ solid angle, indicate that bremsstralung-induced β-γ coincidences are suppressed by more than 10^4 relative to true coincidences.

V. DISCUSSION

Preliminary results from two other measurements of the ^{20}F β-γ correlation have been reported recently. McKeoun *et al.*[15] obtained a slope of $(0.9\pm0.7)\times10^{-3}$ MeV^{-1}, and Rolin *et al.*[16] found $(0.2\pm0.2)\times10^{-3}$ MeV^{-1}. The analysis by Rolin *et al.* assumed that the intercept for the correlation was 1.0 thereby obtaining a small statistical uncertainty for the slope. These new results are in good agreement with our measurement and indicate a much reduced slope from that quoted for Ref. 14. In the following we shall use only the present result since, as we shall find, the uncertainty in extracting the induced currents is not dominated by the uncertainty in the ^{20}F slope determination.

In order to estimate the SCC strength in $A=20$, we shall temporarily neglect the effect of the axial vector second forbidden currents. Thus setting $\Delta(E_0)=0$, Eq. (13) becomes

$$p(^{20}\mathrm{F})-p(^{20}\mathrm{Na})\simeq\frac{E}{2m_nAc}(b-d_{\mathrm{II}})\ . \tag{15}$$

Combining the ^{20}F and ^{20}Na results, we find

$$\left(\frac{b-d_{\mathrm{II}}}{Ac}\right)=8.4\pm1.9\ . \tag{16}$$

Then utilizing the CVC prediction for b/Ac we find the result $d_{\mathrm{II}}/Ac=-0.1\pm2.0$. We can estimate the size of the $\Delta(E_0)j_2$ terms from the wave function predictions for Ref. 24 thus obtaining[25]

$$\frac{3}{2\sqrt{14}}\frac{j_2}{m_nA^2c}\Delta(E_0)=-0.8\ . \tag{17}$$

According to Eq. (13), the strength of the SCC interaction should be modified to $d_{\mathrm{II}}/Ac\approx-0.9\pm2.0$ where only the experimental uncertainties have been included.

The second forbidden interaction included above is not the only one to be reckoned. Another uncertainty is the effect of the quadratic energy dependence of the angular correlation. Because of the low end point energy for the ^{20}F decay, it is difficult to ascertain the quadratic terms directly from experiment. Characterizing the p coefficient to second order as $p=BE+CE^2$, the slope found from a linear fit is $\approx(B+\frac{1}{2}CE_0)$ where E_0 is the end point energy. This is actually an overestimate of the effect of the quadratic terms since in the correlation, the high energy data points have larger uncertainties and thus a smaller weight in the linear least squares fit. C can be obtained either from the ^{20}Na correlation or from the wave function (w.f.) predictions. If we assume that j_2 and j_3 have only first class contributions, then the corrected ^{20}F slope is

$$B(^{20}\mathrm{Na}) = 0.1 \pm 0.9\,, \qquad B(\mathrm{w.f.}) = 0.4 \pm 0.7\,. \tag{18}$$

Thus including both the corrected slope and the contribution from Eq. (17) we obtain $d_{II}/Ac \simeq -0.5 \pm 2.0$ where again no uncertainty has been included for the second forbidden (s.f.) corrections. If we assume a 100% uncertainty for these corrections we find $d_{II}/Ac \simeq -0.5 \pm 2.3$.

The effect of the second forbidden contributions is more serious for the extraction of d_I. From Eq. (14) we note that the j_2 terms for ^{20}F and ^{20}Na add, and hence the correction to the extracted d_I/Ac is about a factor of three larger than was obtained in Eq. (17). Thus the first class induced tensor is

$$\frac{d_I}{Ac}\,(\text{no s.f.}) = 6.6 \pm 2.0\,, \qquad \frac{d_I}{Ac}\,(\text{s.f.}) = 5.0 \pm 2.5\,, \tag{19}$$

where the result quoted for no second forbidden correction was obtained by ignoring j_2 and j_3 while the result with second forbidden correction contains both the $\Delta'(E_0)j_2$ and corrected slope contributions.

Including the second forbidden terms as above assumes that j_2 and j_3 are only first class and therefore are identical in both the electron and positron correlations. It is possible of course that j_2 and j_3 have both first and second class components. In that event the quadratic terms would be different in the two decays and the analysis above would not be valid. We note that observing such a difference would be extremely interesting.

VI. CONCLUSION

The experimental results for the $A = 20$ β-γ angular correlations have been used to determine the strength of recoil order induced weak interactions. Utilizing the G parity transformation property, the first and second class axial vector interactions have been separated. The difference of the two correlations, which depends upon the weak magnetism and SCC interactions, is consistent with CVC and no SCC. However, allowing for possible interference of axial vector second forbidden interactions, only an upper limit of $\frac{1}{3}$ of weak magnetism can be placed on the strength of a SCC interaction. The strength of the first class induced tensor interaction also cannot be extracted unambigously due to the second forbidden contributions. The preliminary result for the first class induced tensor is somewhat larger than the wave function predictions which were calculated with single particle operators obtained via an impulse approximation reduction of the weak currents. A similar discrepancy has been observed in $A = 8$ (Ref. 9) and may be a signal of meson-exchange currents contributing to this interaction.

In order to reduce the uncertainty in both the first and second class induced tensor interactions, it will be necessary to ascertain the role of the second forbidden contributions. The size of the quadratic dependence observed in the ^{20}Na correlation is consistent with the wave function calculations but the uncertainty is rather large. The high end point energy in ^{20}Na accentuates the effect of the second forbidden interactions, thus making it the best candidate to obtain their strength. A more precise measurement than that obtained by the authors of Ref. 18 would provide a somewhat better measure of both the first and second class induced currents since the second forbidden contributions could be reckoned. However, to study the possibility of second class contributions to the second forbidden interactions (especially j_2), the quadratic dependence in both correlations must be measured.

VII. ACKNOWLEDGMENTS

The authors would like to acknowledge the help of D. F. Torgerson and R. D. Macfarlane in the early stages of this experiment. In addition, S. B. Talley and K. Jennings are thanked for their help during data reduction and analysis. The authors are grateful to Rice University for the use of the Tandem Van de Graaff Accelerator at the T. W. Bonner Nuclear Laboratory. This work was supported in part by the National Science Foundation, Robert A. Welch Foundation, and Alfred P. Sloan Foundation.

[1] M. Gell-Mann, Phys. Rev. 111, 362 (1958); R. P. Feynman and M. Gell-Mann, *ibid.* 109, 193 (1958); S. S. Gershtein and J. G. Zeldovich, Zh. Eksp. Teor. Fiz. 29, 698 (1955), [Sov. Phys.—JETP 2, 76 (1957)].
[2] S. Weinberg, Phys. Rev. 112, 1325 (1958).
[3] B. R. Holstein, Rev. Mod. Phys. 46, 789 (1974).
[4] S. Weinberg, Phys. Rev. Lett. 19, 1264 (1967).
[5] See for example S. Weinberg, Phys. Today 30 (No. 4), 42 (1977).
[6] C. S. Wu, Rev. Mod. Phys. 36, 618 (1964).
[7] F. P. Calaprice and B. R. Holstein, Nucl. Phys. A273, 301 (1976).

[8]C. S. Wu, Y. K. Lee, and L. W. Mo, Phys. Rev. Lett. 39, 72 (1977).
[9]R. E. Tribble and G. T. Garvey, Phys. Rev. C 12, 967 (1975); A. M. Nathan, G. T. Garvey, P. Paul, and E. K. Warburton, Phys. Rev. Lett. 35, 1137 (1975).
[10]K. Sugimoto, I. Tanihata, and J. Göring, Phys. Rev. Lett. 34, 1533 (1975).
[11]F. P. Calaprice, S. J. Freedman, W. C. Mead, and H. C. Vantine, Phys. Rev. Lett. 35, 1566 (1975).
[12]P. Lebrun, Ph. Deschepper, L. Grenacs, J. Lehmann, C. Leroy, L. Palffy, A. Possoz, and A. Maio, Phys. Rev. Lett. 40, 302 (1978).
[13]Preliminary measurements with a new experimental geometry indicate that the result for $A=19$ should be modified to no SCC. W. E. Kleppinger, F. P. Calaprice, and D. Mueller, Bull. Am. Phys. Soc. 23, 603 (1978).
[14]F. Boehm, V. Soergel, and B. Steck, Phys. Rev. Lett. 1, 77 (1958).
[15]R. McKeown, F. P. Calaprice, and D. E. Alburger (to be published).
[16]N. Rolin, J. P. Deutsch, D. Favart, M. Lebrun, and R. Prieels, in *Proceedings of the International Conference on Nuclear Structure, Tokyo, 1977*, edited by T. Marumori (Physical Society of Japan, Tokyo, 1978), p. 781.
[17]N. Rolin, J. P. Deutsch, D. Favart, M. Lebrun, and R. Prieels, Phys. Lett. 70B, 23 (1977).
[18]P. D. Ingalls, Nucl. Phys. A265, 93 (1976).
[19]L. K. Fifield, F. P. Calaprice, C. H. Zimmerman, M. J. Hurst, A. Pakkanen, T. J. M. Symons, F. Watt, and K. W. Allen, Nucl. Phys. A288, 57 (1977).
[20]J. D. Pearson and R. H. Spear, Nucl. Phys. 54, 434 (1964).
[21]D. E. Alburger and F. P. Calaprice, Phys. Rev. C 12, 1690 (1975).
[22]D. F. Torgerson, K. Wien, and R. D. Mcfarlane, Phys. Lett. 40B, 203 (1972).
[23]K. Kubodera, J. Delorme, and M. Rho, Nucl. Phys. B66, 253 (1973).
[24]F. P. Calaprice, W. Chung, and B. H. Wildenthal, Phys. Rev. C 15, 2178 (1977).
[25]The phase for j_k reported in Ref. 14 must be modified by $(-1)^{3-k}$, B. R. Holstein (private communication).
[26]F. Ajzenborg-Selove, Nucl. Phys. A300, 1 (1978).